JOURNAL OF GEOPHYSICAL RESEARCH, VOL. 114, A12306, doi:10.1029/2009JA014392, 2009

Temperature enhancements and vertical winds in the lower thermosphere associated with auroral heating during the DELTA campaign

J. Kurihara,[1] S. Oyama,[1] S. Nozawa,[1] T. T. Tsuda,[1] R. Fujii,[1] Y. Ogawa,[2] H. Miyaoka,[2] N. Iwagami,[3] T. Abe,[4] K.-I. Oyama,[5] M. J. Kosch,[6] A. Aruliah,[7] E. Griffin,[7] and K. Kauristie[8]

Received 24 April 2009; revised 27 July 2009; accepted 28 August 2009; published 5 December 2009.

[1] A coordinated observation of the atmospheric response to auroral energy input in the polar lower thermosphere was conducted during the Dynamics and Energetics of the Lower Thermosphere in Aurora (DELTA) campaign. N_2 rotational temperature was measured with a rocket-borne instrument launched from the Andøya Rocket Range, neutral winds were measured from auroral emissions at 557.7 nm with a Fabry-Perot Interferometer (FPI) at Skibotn and the KEOPS, and ionospheric parameters were measured with the European Incoherent Scatter (EISCAT) UHF radar at Tromsø. Altitude profiles of the passive energy deposition rate and the particle heating rate were estimated using data taken with the EISCAT radar. The local temperature enhancement derived from the difference between the observed N_2 rotational temperature and the MSISE-90 model neutral temperature were 70–140 K at 110–140 km altitude. The temperature increase rate derived from the estimated heating rates, however, cannot account for the temperature enhancement below 120 km, even considering the contribution of the neutral density to the estimated heating rate. The observed upward winds up to 40 m s^{-1} seem to respond nearly instantaneously to changes in the heating rates. Although the wind speeds cannot be explained by the estimated heating rate and the thermal expansion hypothesis, the present study suggests that the generation mechanism of the large vertical winds must be responsible for the fast response of the vertical wind to the heating event.

Citation: Kurihara, J., et al. (2009), Temperature enhancements and vertical winds in the lower thermosphere associated with auroral heating during the DELTA campaign, *J. Geophys. Res.*, *114*, A12306, doi:10.1029/2009JA014392.

1. Introduction

[2] Auroral energy deposition in the polar lower thermosphere enhances the neutral temperature directly through Joule and particle heating. An upwelling of heated air is driven by a sudden rise in local temperature and thus vertical winds are generated by intense heating occurring during geomagnetically disturbed conditions [*Smith*, 1998]. Large vertical winds in the lower and upper thermosphere associated with auroral disturbances have been observed by ground-based Fabry-Perot Interferometers (FPIs) since the 1980s [*Rees et al.*, 1984; *Wardill and Jacka*, 1986; *Price and Jacka*, 1991; *Price et al.*, 1995; *Smith and Hernandez*, 1995]. *Price et al.* [1995] measured vertical winds and temperature with a FPI using auroral emissions from atomic oxygen at the wavelengths of 557.7 and 630.0 nm corresponding to the effective emission altitudes of the lower and upper thermosphere, respectively. The observations showed that a large upwelling occurred simultaneously in both altitudes during geomagnetically active conditions and the vertical wind speeds reached 42 m s^{-1} in the lower thermosphere and 138 m s^{-1} in the upper thermosphere. With the large vertical winds, large temperature enhancements of about 200 K in the lower thermosphere were also observed. However, recent FPI observations show that a correlation between the vertical winds in the lower and upper atmosphere does not always exist [*Ishii et al.*, 1999, 2001, 2004; *Kosch et al.*, 2000] and that an apparently inverse relationship between the estimated temperature and auroral intensity is explained by the tendency of the 557.7 nm emission to come from lower heights during bright aurora [*Ishii et al.*, 2001; *Holmes et al.*, 2005]. Although FPIs are valuable tools for simultaneously measuring neu-

[1]Solar-Terrestrial Environment Laboratory, Nagoya University, Nagoya, Japan.
[2]National Institute of Polar Research, Research Organization of Information and Systems, Tokyo, Japan.
[3]Department of Earth and Planetary Science, Graduate School of Science, University of Tokyo, Tokyo, Japan.
[4]Institute of Space and Astronautical Science, Japan Aerospace Exploration Agency, Sagamihara, Japan.
[5]Plasma and Space Science Center, National Cheng Kung University, Tainan, Taiwan.
[6]Communication Systems, Lancaster University, Lancaster, UK.
[7]Atmospheric Physics Laboratory, University College London, London, UK.
[8]Finnish Meteorological Institute, Helsinki, Finland.

0148-0227/09/2009JA014392$09.00

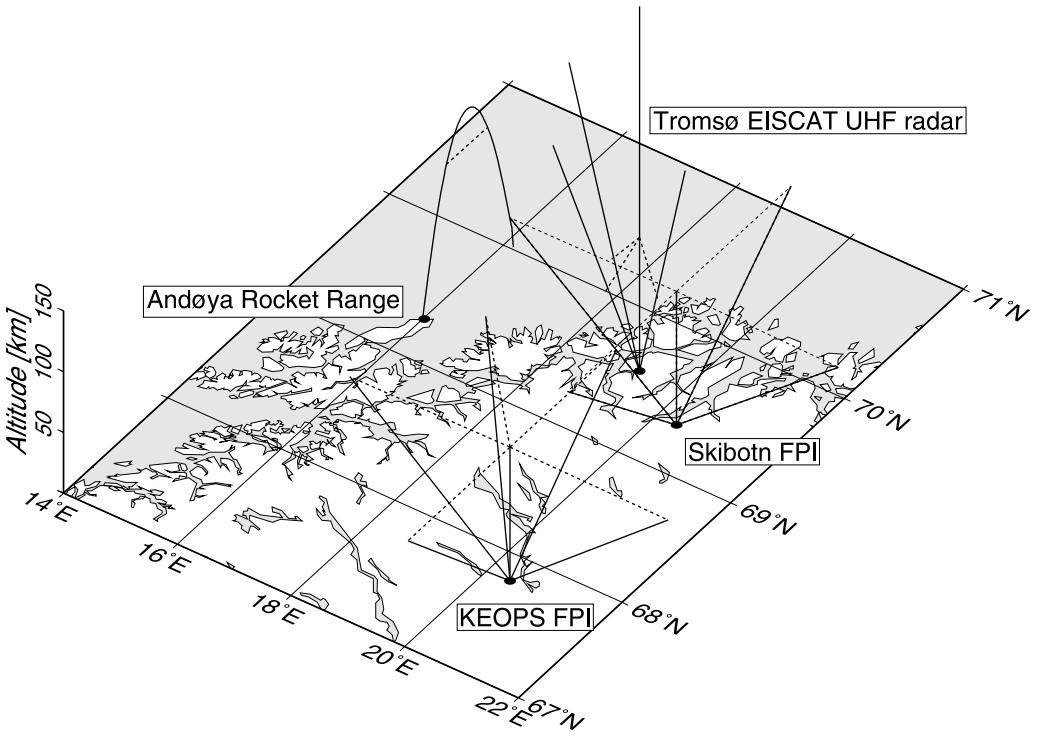

Figure 1. Schematic diagram of the coordinated observation. The solid lines indicate the trajectory of the sounding rocket launched from the Andya Rocket Range and the line of sights of the EISCAT UHF radar at Tromsø and the FPIs at Skibotn and the KEOPS site. The dotted lines present the projection of the solid lines onto the plane at 110 km altitude.

tral wind and temperature, it is difficult for an FPI alone to interpret the connection between vertical winds and temperature enhancements and to identify the source of large vertical winds [*Wescott et al.*, 2006].

[3] In contrast to the FPI observations, only a few studies have attempted vertical wind observations by incoherent scatter (IS) radars in the polar lower thermosphere [*Kofman et al.*, 1996; *Oyama et al.*, 2005, 2008]. The greatest advantage of the IS radar observation in this research issue is that auroral energy deposition can be estimated by the measurements of ionospheric parameters. *Oyama et al.* [2008] measured the vertical neutral wind speed in the lower thermosphere using the European Incoherent Scatter (EISCAT) UHF radar and showed that large upward winds existed in excess of 30 m s^{-1} in association with an auroral heating event.

[4] Modeling studies suggest that large vertical winds driven by local heating in the lower thermosphere have a significant impact on the dynamical and compositional states up to the upper thermosphere [*Walterscheid et al.*, 1985; *Walterscheid and Lyons*, 1992; *Sun et al.*, 1995; *Shinagawa et al.*, 2003; *Shinagawa and Oyama*, 2006]. These regional-scale models, which have the horizontal scale of 100–10,000 km, employ nonhydrostatic simulations to reproduce large vertical winds. *Russell et al.* [2007] indicated that large vertical winds can transport significant amount of molecular nitrogen and oxygen upwards, suggesting that many satellite-borne mass spectrometer measurements may overestimate the concentrations of atomic oxygen during disturbed conditions. Since the nonhydrostatic effects are not included in general circulation models (GCMs), previous GCMs have not been able to reproduce the observed large vertical winds and may have potentially underestimated the upward transport of molecular species [*Smith*, 2000]. More recently, a global-scale nonhydrostatic model was developed [*Deng and Ridley*, 2006a] and the results indicated that the high-latitude Joule heating drives large upward winds of the observed magnitude from the lower altitude source region to higher altitudes [*Deng and Ridley*, 2006b; *Deng et al.*, 2008].

[5] The Dynamics and Energetics of the Lower Thermosphere in Aurora (DELTA) campaign was carried out in December 2004, in order to make a coordinated observation of the thermospheric response against the auroral energy input using a sounding rocket, FPIs, the EISCAT UHF radar, and other ground-based instruments such as all-sky cameras (ASCs) and magnetometers. Figure 1 shows a schematic diagram of the coordinated observation. A multi-instrument investigation of temperature enhancements and vertical winds in the lower thermosphere was one of the main objectives of the DELTA campaign. The preliminary results and detailed description of each instrument have already been published in ten papers as a special issue of Earth, Planets and Space [see the introduction paper by *Abe et al.*, 2006]. The vertical profile of neutral temperature in the lower thermosphere was obtained by the sounding rocket experiment [*Kurihara et al.*, 2006], time variations of neutral temperature and winds at the auroral emission altitudes were measured with two FPIs at Skibotn and at the KEOPS (Kiruna Esrange Optical Platform Site) [*Griffin et al.*, 2006], and the altitude and temporal profiles of ionospheric parameters and neutral winds were observed by the

EISCAT UHF radar [*Nozawa et al.*, 2006]. Although these studies have made comparisons with the observational results of other instruments, a comprehensive study focused on temperature enhancements and vertical winds in the context of auroral heating has not been reported for the DELTA campaign. Since it is very difficult to obtain an altitude profile of neutral temperature in the lower thermosphere, these data sets provide more unique and valuable information than ever before. In the present paper, possible causes of temperature enhancements and vertical winds observed with the rocket-borne instrument and the Skibotn FPI in the lower thermosphere during the DELTA campaign are discussed by estimating auroral heating rates quantitatively using data taken with the EISCAT UHF radar.

2. Observations

2.1. In Situ Temperature Observation

[6] During the DELTA campaign, a Japanese sounding rocket S-310-35 was launched from the Andøya Rocket Range (69.3°N, 16.0°E geographic coordinates) in Norway, at 00:33 UT, 13 December 2004, under geomagnetically disturbed conditions when the three hourly geomagnetic Kp index was 4+ for 00:00–03:00 UT. The Andøya Rocket Range is located at 67.4°N, 113.4°E geomagnetic coordinates and the Magnetic Local Time (MLT) is given by UT + 2.5 hours. A total of eight scientific instruments on the rocket carried out successful measurements [*Abe et al.*, 2006]. Rotational temperature and number density of atmospheric molecular nitrogen (N_2) were observed with the N_2 Temperature of Vibration (NTV) instrument installed on the rocket [*Kurihara et al.*, 2006]. The instrument used the Electron Beam Fluorescence (EBF) technique and consisted of an electron gun to excite and ionize the ambient N_2 and a spectrometer to detect the fluorescence of the N_2^+ first negative (1N) system. The N_2 rotational temperature was determined by fitting a synthetic spectrum to the measured spectrum of the N_2^+ 1N (0, 0) band at 391.4 nm and the number density was calculated from the intensity of the band [*Kurihara and Oyama*, 2005].

[7] The sounding rocket flew geographically northward from Andøya and reached an apogee of 140.0 km at 184 s from the launch. The N_2 rotational temperature and number density measurements by the NTV were conducted at 97–140 km altitude during the ascent of the rocket flight and 140–95 km during the descent. The rotational temperature of N_2 is expected to be equal to the neutral temperature in the lower thermosphere, because the equilibrium between rotational and translational degrees of freedom for N_2 is immediately established by the high collision frequency of the lower thermosphere. The relaxation time for attaining the equilibrium is $\sim 10^{-3}$ s at 95 km altitude and $\sim 10^{-1}$ s at 140 km [*Kurihara et al.*, 2006]. Such a short relaxation time ensures that N_2 rotational temperature can be used as a proxy of neutral temperature even during an auroral heating event in the polar lower thermosphere. However, below 110 km, the rotational temperature measured by the NTV might not be equal to the ambient neutral temperature because of the aerodynamic effects around the rocket at supersonic speed. Since the measurement volume of the NTV was located in the vicinity of the payload, N_2 molecules passing through the shock front could enter the measurement volume. If the travel time from the shock front to the measurement volume was longer than the relaxation time, the measured rotational temperature could be higher than the ambient atmospheric temperature. *Kurihara et al.* [2006] has demonstrated that the rotational temperature measurement was free from the aerodynamic effects above 110 km, as expected theoretically. It should also be noted that horizontal distance between the ascent and the descent varied with altitude owing to the rocket trajectory. The horizontal distances were 40, 33, and 22 km at 110, 120, and 130 km altitudes, respectively.

[8] Figure 2a shows altitude profiles of the observed N_2 rotational temperature during the ascent and descent of the rocket flight. The observed rotational temperatures in the ascent and descent agree well above 110 km. Below that altitude, rotational temperature measurements were affected by the aerodynamic effects and are not plotted here to avoid confusion.

[9] The difference between the observed N_2 rotational temperature and the neutral temperature predicted by the Mass Spectrometer Incoherent Scatter (MSISE-90) model [*Hedin*, 1991] is 70–140 K as shown in Figure 2b. Since the empirical MSIS model uses a planetary geomagnetic index Ap as an input parameter, the MSIS model value intrinsically represents the mean state of the upper atmosphere for the global-scale geomagnetic activity. Figure 2a also shows the MSIS model neutral temperature calculated using the variation of three hourly geomagnetic index ap during the previous 48 hours, instead of daily index Ap. The neutral temperature profile derived using the ap variation is slightly higher than that using the daily Ap but much lower than the observed N_2 rotational temperature.

[10] In addition, the ion temperature observed by the EISCAT UHF radar about two hours before the rocket launch is shown in Figure 2a and the difference between the ion temperature and the MSIS model temperature is plotted in Figure 2b. The ion temperature at each altitude is averaged temporally for 22:30–23:00 UT and spatially for four sampling positions. As shown in the next section, the EISCAT UHF radar and magnetometer observations indicate that ionospheric condition was geomagnetically quiet during 22:20–23:20 UT. The ion temperature in the lower ionosphere is expected to be close to the neutral temperature during such quiet conditions. The observed ion temperature is higher than the MSIS model neutral temperature above 110 km but lower than the observed N_2 rotational temperature.

[11] Therefore, it is considered that the temperature difference between the observed N_2 rotational temperature and the MSIS model neutral temperature or the EISCAT quiet time ion temperature is a temperature enhancement caused by the local heating. The validity of the N_2 rotational temperature measurement has already been discussed by *Kurihara et al.* [2006] and the assumption of local heating is a subject of discussion in the present study.

2.2. EISCAT UHF Radar Observation

[12] The EISCAT UHF radar observations at Tromsø (69.6°N, 19.2°E geographic coordinates; 67.1°N, 116.4°E geomagnetic coordinates) in Norway were conducted on 5 and 8–13 December 2004 during the DELTA campaign [*Nozawa et al.*, 2006]. In most of the observations, the

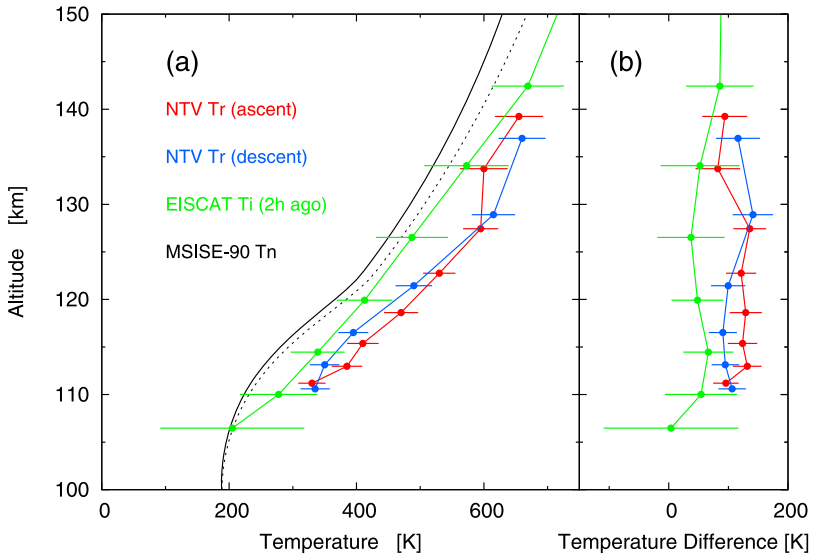

Figure 2. Altitude profiles of (a) the N_2 rotational temperature observed by the NTV instrument during the ascent (red) and descent (blue) of the rocket flight, compared with the neutral temperature from the MSISE-90 model (black) and the ion temperature observed by the EISCAT UHF radar two hours before the rocket launch (green), and (b) temperature differences between the MSISE-90 model and the N_2 rotational temperature during the ascent (red), the MSISE-90 model and the N_2 rotational temperature during the descent (blue), and the MSISE-90 model and the EISCAT ion temperature (green). The dotted line indicates the MSIS-E-90 model neutral temperature using three hourly index ap variation, instead of daily index Ap.

EISCAT UHF radar was operated in a Common Program 2 (CP2) mode in which the line of sight of the combined transmitter and receiver antenna was pointed to four consecutive directions, including one field aligned position, with a dwell time of ~1 min in each position, making a full cycle time of 6 min. In addition to the electron density, electron temperature, and ion temperature, which are derived from each position, the three-dimensional ion velocity vectors are derived every 6 min by combining three sets of line-of-sight velocities from ~90 km to ~500 km altitude. From these ion velocity vectors, the electric field vectors can be derived assuming that the *F* region plasma drifts perpendicular to the geomagnetic field are solely due to the electric field. The electric field **E** is then obtained by

$$\mathbf{E} = -(\mathbf{v} \times \mathbf{B}), \quad (1)$$

where **v** is the ion velocity at 282 km and **B** is the geomagnetic field derived from the International Geomagnetic Reference Field (IGRF) model.

[13] The EISCAT UHF radar observation at Tromsø suggests the presence of a strong auroral heating associated with the geomagnetic disturbance around the time of the rocket launch. Figure 3 summarizes the time variation of parameters observed by the EISCAT UHF radar and a ground-based magnetometer at Tromsø. Figure 3a shows the horizontal component of the geomagnetic field (H component) observed by the magnetometer. The H component immediately decreased by 200 nT in the interval of 00:00–00:10 UT, about half an hour prior to the rocket launch at 00:33 UT and two hours after a sudden southward turning of the interplanetary magnetic field (IMF)-Bz component recorded by the ACE spacecraft at 22:07 UT [*Abe et al.*, 2006]. Data from ground-based magnetometers in the IMAGE (International Monitor for Auroral Geomagnetic Effects) network suggest that the horizontal ionospheric current was flowing westward for the time interval from 00:00 to 03:30 UT over a meridionally wide region including Sørøya (70.5°N, 22.2°E) and Pello (66.9°N, 24.1°E). Figure 3b indicates the meridional and zonal components of the electric field strength observed by the EISCAT UHF radar. The southward electric field at 50 mV m^{-1} lasted for an hour before the rocket launch. Figures 3c and 3d show the height variation of the electron density and ion temperature in the *E* region, respectively. The electron density was very low from 23:40 to 00:10 UT due to evacuation of the ionospheric electrons in association with the downward field-aligned current. After 00:10 UT the electron density was enhanced by the precipitation up to $\sim 10^{11}$ m^{-3} all over the *E* region. The enhancement of the electron density raised the ionospheric conductivity. The ion temperature above 120 km increased several hundred K in response to the large increase in the electric field. The enhancement of the electric field coupled with the enhancement of the ionospheric conductivity enhances Joule heating in the lower thermosphere.

[14] *Nozawa et al.* [2006] derived neutral temperature from the ion temperature observed with the EISCAT UHF radar at the field-aligned direction from 00:35:15 to 00:36:00 UT, a time interval during the ascent of the rocket flight. The derived neutral temperature showed reasonable agreement with the observed rotational temperature but better agreement with the MSIS neutral temperature. The cause of these results is mainly attributable to variability of the observed ion temperature. As shown in Figure 3d, the

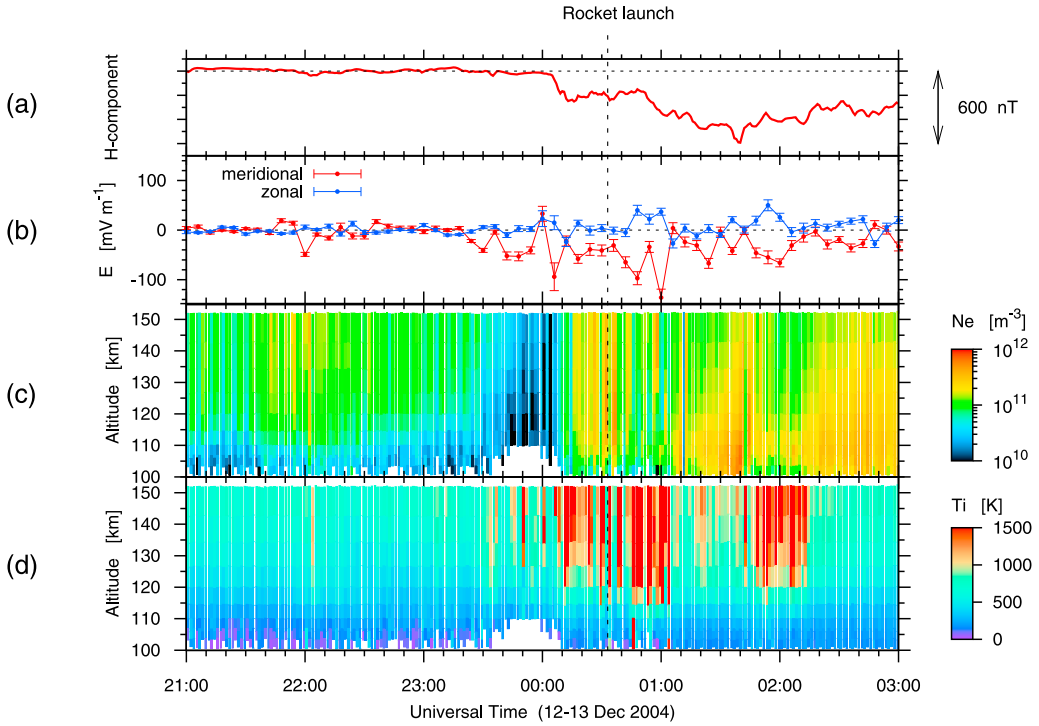

Figure 3. The EISCAT UHF radar and the magnetometer observation at Tromsø, showing (a) the horizontal component of the geomagnetic field, (b) the meridional (red line) and zonal (blue line) components of the electric field strength, (c) the electron density, and (d) the ion temperature in the *E* region.

observed ion temperature was highly variable and the ion temperature at 00:35:15–00:36:00 UT was relatively low compared with the other observation periods around the rocket flight. For example, the ion temperature at 114 km varied from 400 to 900 K during 10 minutes between 00:30 and 00:40 UT. Such large variation of the ion temperature data in this period was also shown by *Griffin et al.* [2006]. As pointed out by *Nozawa et al.* [2006], the considerable variation in the ion temperature would be caused by variation in the electric field associated with moving auroral structures. Note that the electric field in Figure 3b was not as variable as the ion temperature because the electric field was deduced from a six minute cycle of the ion velocity measurements.

2.3. Ground-Based Optical Observations

[15] For the DELTA campaign, the FPIs at Skibotn (69.3°N, 20.4°E) in Norway and at the KEOPS (67.8°N, 21.0°E) in Sweden sampled the 557.7 nm green line emission and provided neutral temperatures and line-of-sight wind velocities [*Griffin et al.*, 2006]. Both the FPIs scanned in the zenith and the four cardinal directions, the KEOPS FPI also scanned in the northwestward direction. The Skibotn FPI used an integration time of 10 s for each direction resulting in a cycle time of about 7 min 20 s and the KEOPS FPI took an integration time of 30 s resulting in a cycle time of 8 min. Since FPIs are passive optical instruments, the observed neutral temperature and wind speed are intensity-weighted mean values along the line of sight and thus approximately equal to the values at the peak emission altitude.

[16] *Griffin et al.* [2006] found an apparent wind divergence and upward vertical winds from the green line observation by the FPI at Skibotn around the time of the rocket launch. There was the apparent divergence in the line-of-sight velocities in the cardinal directions around 00:00–01:00 UT, showing opposite velocities in the northward and southward directions and also in the eastward and westward directions. The "apparent divergence" may be caused by the failure of the standard assumption that the line-of-sight neutral wind velocity consists of only a horizontal component, or caused by the presence of cloud scatter. The all-sky camera shows clear skies during the rocket launch, thus it is likely that there was a significant vertical wind component distorting the FPI analysis.

[17] Figure 4a shows vertical wind speeds measured in the zenith direction of the Skibotn FPI. At Skibotn cloudy conditions were observed until 21:36 UT, which generally render the wind observations from the FPIs based on Doppler shifts unreliable. Some measurements in the clear conditions after 21:36 UT were also slightly inaccurate mainly due to the low intensity of the green line emission. Except for the periods of unreliable measurements before 21:36 UT and less accurate measurements with large error bars, significantly upward vertical winds up to 40 m s^{-1} were observed around 22:00 UT and 00:00–01:00 UT. A wind speed of 40 m s^{-1} is unusually large for a vertical wind in the lower thermosphere and such large vertical winds have been observed only under highly disturbed conditions even in the auroral region [see *Smith*, 1998, and references therein]. On the other hand, significantly downward vertical winds in excess of 20 m s^{-1} were

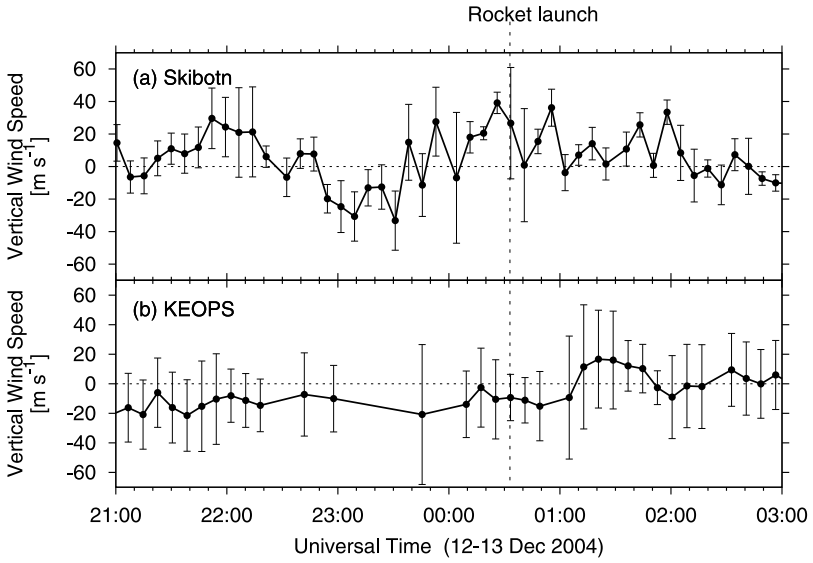

Figure 4. Time variations of the vertical winds from the green line observation with the FPIs at (a) Skibotn and (b) the KEOPS, where positive wind speed is indicated upward.

observed around 22:50–23:30 UT. The zero baselines of the vertical wind speed are usually determined by assuming that the long term average vertical wind is zero and a systematic error in excess of 10 m s^{-1} may occur in geomagnetically disturbed conditions [*Aruliah and Rees*, 1995]. Although this means that the zero vertical wind baseline used in the Skibotn FPI observation could suffer the same problem, the vertical wind observations in the 00:00–01:00 UT and 22:50–23:30 UT periods demonstrated the most positive and negative wind speeds in that night, respectively [*Griffin et al.*, 2006]. Figure 4b shows vertical wind speeds measured with the KEOPS FPI. At the KEOPS site clear conditions were observed throughout the night. Since the intensities of the green line emission measured in the zenith direction of the KEOPS FPI were lower than those of the Skibotn FPI in the 22:30–03:00 UT period, the measurement errors for the vertical wind speed were relatively large for the KEOPS. The KEOPS vertical wind speeds showed little variation and were around 10 m s^{-1} downward during the 00:00–01:00 UT period. This indicates that the large upward winds seen by the Skibotn FPI are very localized. The localized nature of upward vertical winds is important because hydrostatic equilibrium cannot support large vertical winds over hundreds of kilometers distance, which is why the standard GCMs do not show large vertical winds.

[18] The ground-based ASCs have observed intense auroral emissions for over 30 minutes around the rocket flight. During the flight, vortical auroral structures elongated in the east-west directions were propagating eastward with a speed of 2–3 km s^{-1} over the region between 68 and 70°N [see *Kurihara et al.*, 2006, Figure 1]. Figure 5 shows the green line emissions observed by the ASC at Kilpisjärvi (69.0°N, 20.9°E), a site of the Magnetometers-Ionospheric Radars-All-sky Cameras Large Experiment (MIRACLE) network. *Kurihara et al.* [2006] determined the effective altitude of auroral structures during the rocket flight by combining two ASC images at 557.7 nm obtained from two separate stations, Kilpisjärvi and Muonio (68.0°N, 23.5°E). The resultant peak altitude of green line emission was about 120 km. They found that the neutral temperature of about 500 K from the FPI 557.7 nm measurements was consistent with the observed N_2 rotational temperature at 120 km altitude rather than the MSIS model value at that altitude. This agreement also supports the validity of the rotational temperature measurement.

3. Auroral Heating Rate Estimation

[19] In order to investigate the relationship between auroral energy inputs, temperature enhancements, and the vertical winds, auroral heating rates are estimated using data taken with the EISCAT observations. The Joule heating induced by ionospheric current **J** and the particle heating deposited by precipitating electrons have direct heating effects on the neutral atmosphere.

[20] The Joule heating rate $q_J = \mathbf{J} \cdot \mathbf{E}'$ can be expressed as [*Brekke*, 1997; *Fujii et al.*, 1999]

$$\mathbf{J} \cdot \mathbf{E}' = \sigma_P (\mathbf{E}')^2 = \sigma_P (\mathbf{E} + \mathbf{U} \times \mathbf{B})^2, \tag{2}$$

where σ_P is the Pedersen conductivity, **U** is the neutral wind velocity, and $\mathbf{E}'$ is the electric field in the reference frame of the neutral wind. If the electric field strength is sufficiently large and the neutral wind speed is negligibly small, the Joule heating rate can be approximated by the passive energy deposition rate, $q_J^E = \sigma_P E^2$. The present study uses the passive energy deposition rate as an indicator of the Joule heating rate for simplicity. The inclusion of the neutral wind dynamo is discussed later. The Pedersen conductivity can be expressed as [*Brekke and Hall*, 1988; *Brekke*, 1997]

$$\sigma_P = \frac{N_e e}{B} \left(\frac{\Omega_e \nu_{en}}{{\Omega_e}^2 + {\nu_{en}}^2} + \frac{\Omega_i \nu_{in}}{{\Omega_i}^2 + {\nu_{in}}^2} \right), \tag{3}$$

where N_e is the electron density, e is the electron charge, Ω_e and Ω_i are the electron and ion gyrofrequencies, respectively, and ν_{en} and ν_{in} are the electron-neutral and ion-

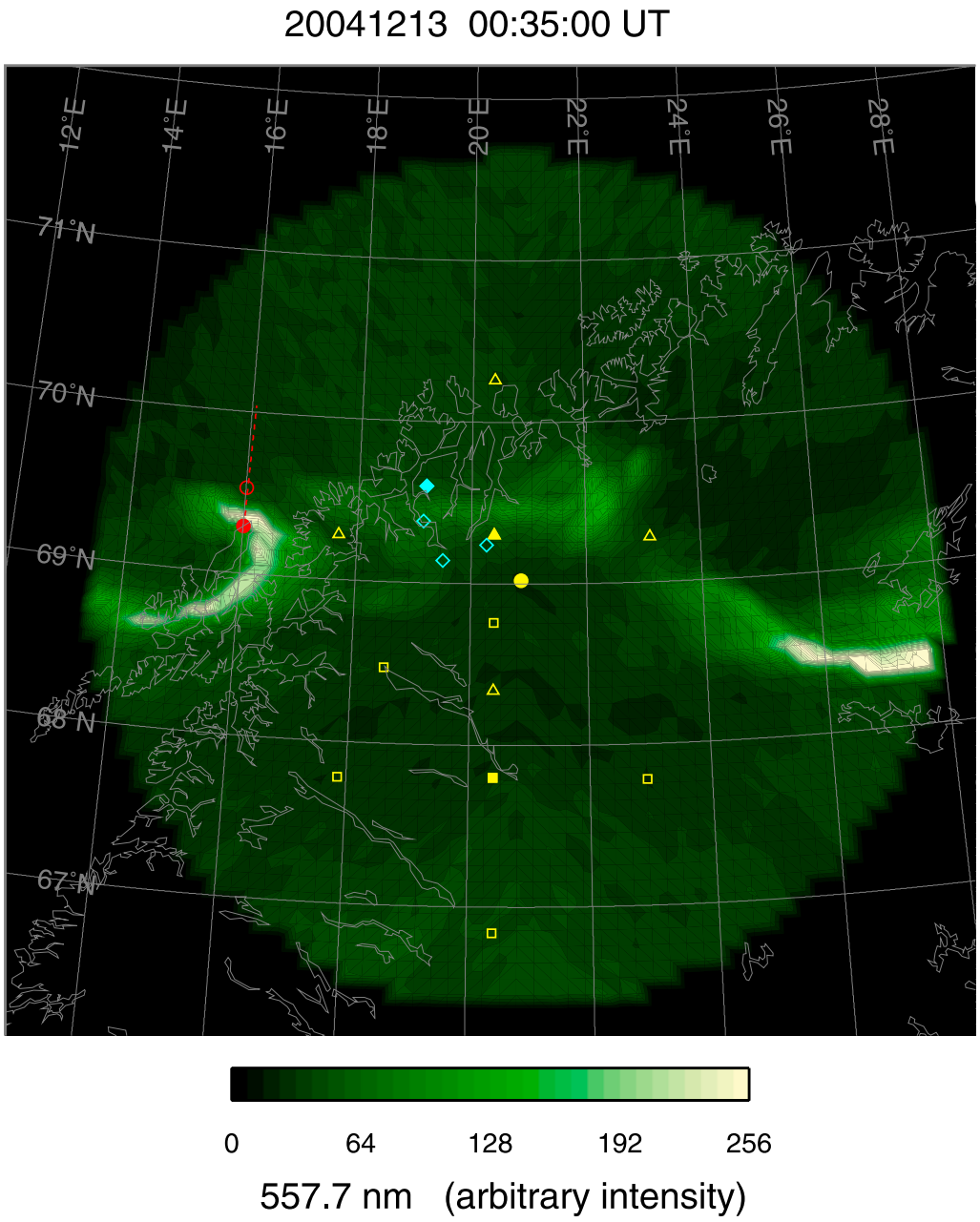

Figure 5. The ASC image of 557.7 nm emission observed at Kilpisjärvi (solid yellow circle) at 00:35:00 UT on the projected altitude of 110 km. The sounding rocket (open red circle) launched from Andya Rocket Range (solid red circle) was at an altitude of 120 km during the ascent of the flight. The sampling positions of the EISCAT UHF radar at Tromsø (blue diamonds), the Skibotn FPI (yellow triangles), and the KEOPS FPI (yellow boxes) are mapped to 110 km altitude, expressing their zenith positions in solid symbols.

neutral collision frequencies, respectively. These parameters needed for calculation of the Pedersen conductivity are derived from the EISCAT observation and the MSISE-90 model. The Pedersen conductivity is integrated from 100 to 300 km to derive the height-integrated passive energy deposition rate, $Q_J^E = \int q_J^E dh = E^2 \int \sigma_P dh$.

[21] The particle heating rate q_p can be written as [*Vickrey et al.*, 1982]

$$q_p = \epsilon \alpha_{eff} N_e{}^2, \tag{4}$$

where ϵ is the energy per ion-electron pair, which is deposited in the atmosphere as heat, and α_{eff} is the effective recombination coefficient. It is assumed that the ionization rate is equal to the recombination rate, $\alpha_{eff} N_e^2$. The effective recombination coefficient ($m^3\ s^{-1}$) is given as a function of height h (km) above 85 km by

$$\alpha_{eff} = 2.5 \times 10^{-12} \exp\left(-\frac{h}{51.2}\right), \tag{5}$$

based on the various measurements [*Vickrey et al.*, 1982]. The particle heating rate is calculated on the assumptions

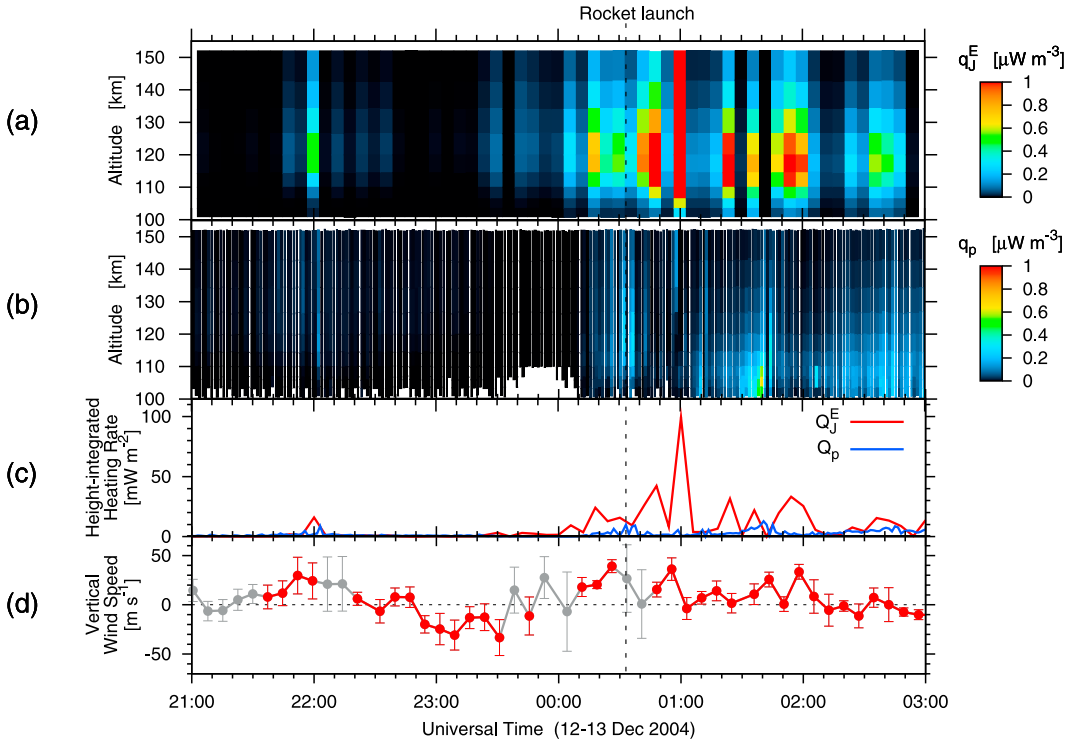

Figure 6. Time variations of the auroral heating rates observed by the EISCAT UHF radar, showing (a) the passive energy deposition rate, (b) the particle heating rate, and (c) their height-integrated values. (d) The same as Figure 4a, but the unreliable measurements due to the cloudy conditions before 21:36 UT and the less accurate measurements with error bars larger than 20 m s^{-1} are represented in gray and the other in red.

that (1) steady state conditions hold during the data integration period, (2) ion transport can be ignored ($h <$ 160 km), (3) no source of ionization exists other than particle precipitation, and (4) ϵ = 35 eV are expended per ion-electron pair. The height-integrated particle heating rate, $Q_p = \int q_p dh$, is integrated from 95 to 160 km.

[22] Figures 6a and 6b illustrate the time variations of q_J^E and q_p, respectively, per unit volume (μW m^{-3}) between 100 and 150 km and Figure 6c shows the time variations of Q_J^E and Q_p per unit area (mW m^{-2}). Excluding the interval of 21:50–22:10 UT, Q_J^E and Q_p were very small until 00:00 UT. Q_J^E increased from 00:00 UT, 33 minutes before the rocket launch, because of the enhancements both in the electric field strength and the electron density. Although the electric field magnitudes up to 50 mV m^{-1} from 23:20 to 00:00 UT were similar to those from 00:00 to 00:40 UT as shown in Figure 3b, Q_J^E from 23:20 to 00:00 UT were much smaller than those from 00:00 to 00:40 UT due to the low electron density in the E region. Q_J^E was relatively steady until 00:40 UT and continued intermittently for hours after that. The altitude profile of q_J^E, which depends on the Pedersen conductivity, shows a peak around 120 km. Q_p also increased from 00:00 UT with the enhancement in the electron density. While Q_p was mostly lower than Q_J^E until 00:30 UT, they were comparable during the rocket flight. The peak altitude of q_p was 115–120 km around the period of the rocket launch and 105–110 km after 01:00 UT. *Iwagami et al.* [2006] estimated the characteristic energy of the precipitating auroral electrons during the rocket flight to be 4 keV, by comparing the observed peak altitude of the green line emission [*Kurihara et al.*, 2006] with the calculated green line volume emission rate for unit incident flux [*Banks et al.*, 1974]. The peak altitudes of q_p during the rocket flight are consistent with the calculated ionization rate for the characteristic energy of 4 keV that peaks around 120 km [*Banks et al.*, 1974].

[23] Since the first presentation by *Brekke and Rino* [1978] regarding the altitude profiles of the Joule heating rate with the observed E region neutral winds, the influence of the neutral wind on the electromagnetic energy deposition in the polar lower thermosphere has been examined in a number of studies using IS radar observations [*Fujii et al.*, 1998, 1999; *Thayer*, 1998a, 1998b, 2000; *Fujiwara et al.*, 2004]. The use of the passive energy deposition rate as an indicator of the Joule heating rate is valid if the neutral wind effect $\mathbf{U} \times \mathbf{B}$ is negligible compared with the electric field $\mathbf{E}$ in Equation (2). Although the E region neutral wind data derived by the EISCAT UHF radar is available in this campaign, the data shows rapid and scattered temporal variations during 21:00–02:00 UT and needs careful treatment [*Nozawa et al.*, 2006]. The temporal variations of the neutral wind is possibly caused by temporal variations of the electric field, which also affected the temporal variations of the ion temperature as already mentioned in Section 2.2. Meanwhile, the FPI wind measurements show horizontal neutral winds less than 100 m s^{-1} [*Griffin et al.*, 2006]. This horizontal wind data, which were derived assuming no vertical component in the line-of-sight velocities, provide upper limits for horizontal wind speeds at the effective altitudes of the 557.7 nm emission. Assuming that $|\mathbf{U}|$ is

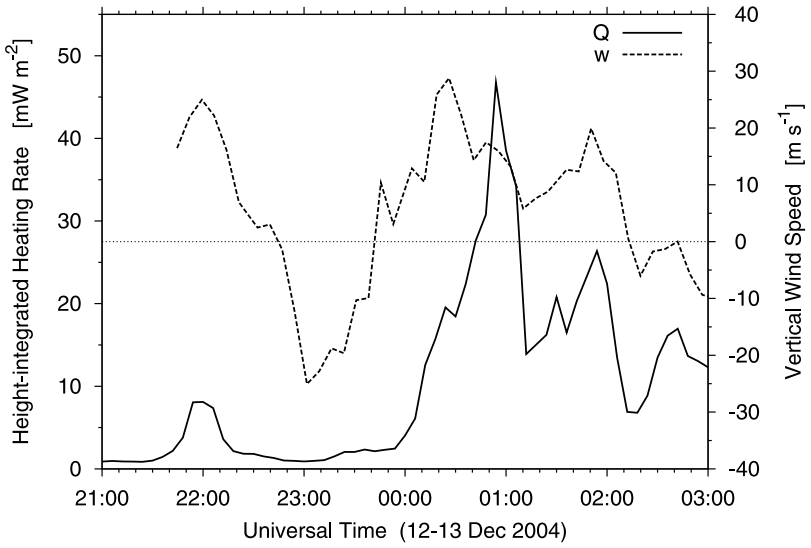

Figure 7. Time variations of the height-integrated heating rate (solid line) and vertical wind speed (dashed line) smoothed using a three point running average.

100 m s^{-1} and **B** is perpendicular to **U**, the maximum magnitude of the neutral wind induced electric field $|\mathbf{U} \times \mathbf{B}|$ is estimated to be ~4.5 mV m^{-1}. Therefore the contribution of the neutral wind to the Joule heating rate is less than ~10% during the interval of 00:00–00:30 UT when the strong electric field of 50 mV m^{-1} level was observed.

[24] Another source of ambiguity in the auroral heating rate estimation is the neutral density. The particle heating rate estimation depends on the ion density and not on the neutral density; but the Joule heating rate and the passive energy deposition rate depends on the neutral number density through ν_{en} and ν_{in} in the calculation of σ_P. The influence of the neutral density on the Joule and passive energy deposition rates are significant below about 120 km, where ν_{in} is larger than Ω_i, and the Joule and passive energy deposition rates are almost in inverse proportion to the neutral number density below 110 km. Since ν_{in} is calculated using the neutral number density from the MSISE-90 model, the derived auroral heating rate below 120 km is underestimated (overestimated) if the local neutral density is lower (higher) than the MSISE-90 model value.

4. Discussion

4.1. Vertical Winds

[25] From Figure 6, it becomes clear that the positive vertical wind speed is associated with the estimated auroral heating rates. In addition, the time response of the upward vertical wind to the auroral heating seems to be very fast and at least comparable to the time interval between vertical wind measurements, judging from the onset of the auroral heating event around 22:00 and 00:00 UT and the variation with timescale of less than about 15 minutes in the interval of 00:00–02:00 UT. The upward vertical winds around 22:00 UT and during 00:00–02:00 UT seem to respond to the increase of Q_J^E rather than that of Q_p owing to a relatively larger contribution of Q_J^E to the total heating rate.

[26] In order to more clearly show a relationship between the vertical wind speed and the heating rate in Figure 6, the data smoothed using a three point running average during 21:00–03:00 UT are shown in Figure 7. The vertical wind data for the cloudy condition before 21:36 UT are not used for smoothing, and the height-integrated heating rate is the sum of Q_J^E and Q_p. There seems to be a positive relationship between the vertical wind speed and the height-integrated heating rate and an almost instantaneous response of the vertical wind speed to the height-integrated heating rate in this timescale. It should be mentioned, however, that a peak of vertical wind speed at 00:26 UT precedes a peak of the height-integrated heating rate by 30 minutes. This deviation is possibly attributable to horizontal difference of the measurement regions covered with the EISCAT UHF radar and the Skibotn FPI. While vertical wind speeds were measured in the small field of view of the Skibotn FPI, electron densities and ion velocity vectors used for calculating the heating rates were sampled in the four separated directions from the EISCAT UHF radar as shown in Figures 1 and 5. It is suggested from the electron densities and ion temperatures in Figure 3 and the all-sky camera images as in Figure 5 that the heating rates were not horizontally uniform in the measurement region of the EISCAT UHF radar during 00:00–01:00 UT, and that the estimated heating rates in this period may not be proportional to the actual heating rates in the measurement region of the Skibotn FPI. The heating rates in the other periods are suggested to be horizontally uniform in the measurement region of the EISCAT UHF radar because the electron densities and ion temperatures are similar in the four directions.

[27] It should be noted that the altitude at which the vertical wind was measured may have varied during this time period. The effective altitude of the auroral green line emission at 00:34–00:37 UT was determined to be about 120 km from the ASC observations [*Kurihara et al.*, 2006]. Then, the neutral temperature by the Skibotn FPI 557.7 nm observation showed a sharp drop from 500 K to 400 K level after 01:00 UT [*Griffin et al.*, 2006], suggesting a decrease of the green line emission height down to about 110 km. This result also suggests an increase of the characteristic energy of precipitating auroral electrons and lowering of the peak altitude of q_p, and in fact, the peak altitudes of q_p

and q_J^E were 105–110 km and 120 km, respectively, in the interval of 01:30–01:45 UT when upward vertical winds up to 30 m s^{-1} were observed.

[28] These results support the suggestion by *Price and Jacka* [1991] that large upward winds of 30 m s^{-1} at altitudes higher than 110 km are produced by a combination of Joule and particle heating, while large upward winds at lower altitudes are the consequence of particle heating below that height. Their suggestion is based on FPI 557.7 nm observations with a partial reflection radar observation for enhanced ionization in the *D* region. However, they have not obtained actual auroral heating rates. *Oyama et al.* [2008] compared the height-resolved vertical winds with the height-integrated auroral heating rates using a tristatic experiment with the EISCAT UHF radar. They found large upward winds in excess of 30 m s^{-1} at 109, 114, 120 km altitudes in association with a heating event and large downward winds in excess of −30 m s^{-1} before and after the heating event. Although their result is similar to the present result in several points such as magnitudes of the vertical winds and auroral heating rates, they have not discussed the altitude profile of the auroral heating rates.

[29] It should also be noted that the large downward winds in excess of −20 m s^{-1} were observed during 22:50–23:30 UT. Although large downward winds in the lower and upper thermosphere have often been observed at the equatorward side of an auroral arc [*Crickmore et al.*, 1991; *Innis et al.*, 1997; *Ishii et al.*, 2001], there is no plausible explanation for the large downward winds [*Ishii et al.*, 2001]. There may be a simple explanation that upward winds must be compensated by downward winds to keep the atmosphere from disappearing. However, it is difficult to find a counterpart to the observed downward winds because of the horizontal motion. In the present observation the large downward winds were found in a period of very low heating rate as shown in Figure 6 and the altitude of the large downward winds is unknown because the emission altitude cannot be estimated in this period. The explanation for the large downward winds is an important issue to be studied in the future.

[30] Upward vertical winds generated by the thermal expansion due to heating can be estimated using the first law of thermodynamics

$$w = \frac{q}{\rho\left(C_p \frac{dT}{dz} + g\right)}, \tag{6}$$

where w is the vertical wind speed, q is the total heating rate, ρ is the neutral mass density, C_p is the specific heat at constant pressure, T is the neutral temperature, and g is the acceleration due to gravity [*Hays et al.*, 1973]. The values of ρ and C_p are calculated from the MSISE-90 model density and composition. The vertical temperature gradient dT/dz is 15 K km^{-1} at 120 km from the observed temperature profile and this value is not much different from the MSISE-90 model temperature gradient of 18 K km^{-1} at 120 km. The derived vertical wind speed is ∼2 m s^{-1} at 120 km, when the heating rate is 0.5 μW m^{-3}. This result demonstrates that the estimated heating rate is at least one order of magnitude smaller than that required to generate the observed vertical wind speed by thermal expansion.

[31] Most of the previous studies have indicated that the estimated heating rate is one order of magnitude smaller than the required heating rate for the observed large upward winds in the lower thermosphere [*Wescott et al.*, 2006; *Oyama et al.*, 2008]. A highly complicated nonhydrostatic model also faced the problem of lower speed of the simulated vertical wind than the observed magnitude in the lower thermosphere [*Shinagawa et al.*, 2003]. On the other hand, some recent models succeeded in reproducing large upward winds of the observed magnitude in the upper atmosphere [*Russell et al.*, 2007; *Deng et al.*, 2008].

[32] The present study quantified the temporal response of the vertical winds to the auroral heating event and the relative importance of Joule and particle heating to vertical winds at each altitude using the data independently observed with the FPI and the EISCAT UHF radar. The response time of vertical winds to the auroral heating event seems to be very fast and at least comparable to the sampling interval of the vertical winds, 7 min 20 s. This result suggests the generation mechanism of large vertical winds could respond instantaneously to changes in the auroral heating rate. Although the observed vertical wind speeds cannot be explained by the observed heating rate and the thermal expansion hypothesis, the thermal expansion remains a potential mechanism that can respond rapidly to changes in the auroral heating rate.

4.2. Temperature Enhancements

[33] The auroral heating event studied here gave a good opportunity to estimate the temperature enhancement by auroral heating, because the strong heating event started suddenly after the long duration of low heating rates. Figure 8a shows the altitude profile of the average auroral heating rates from 00:03 to 00:33 UT. In this period, the averaged q_J^E was 4–10 times larger than the averaged q_p and their total heating rate had a peak of 0.5 μW m^{-3} at 120 km altitude.

[34] The temperature increase rate can be estimated by dividing the heating rate by the specific heat and the mass density of the neutral atmosphere

$$\frac{\partial T}{\partial t} = \frac{q}{\rho C_p}. \tag{7}$$

The value of ρ is calculated from the MSISE-90 model density. Figure 8c shows the derived temperature increase rates and, for the purpose of reference, Figure 8b shows the average auroral heating rates per unit weight, q/ρ. Although the total heating rate per unit volume in Figure 8a peaks at 120 km and decreases above that height, the temperature increase rate in Figure 8c monotonically increases with altitude in the lower thermosphere. This is because the mass density decreases more rapidly than the heating rate, as is clearly seen from Figure 8b. These results seem inconsistent with the uniform temperature difference of 70–140 K between the observed N_2 rotational temperature and the MSIS model neutral temperature at 110–140 km altitude in Figure 2b. There are also significant differences between the observed N_2 rotational temperature and the EISCAT quiet time ion temperature, particularly in 112–128 km altitude during the ascent. If the auroral heating event had started from 00:03 UT and lasted for 30 minutes until the rocket

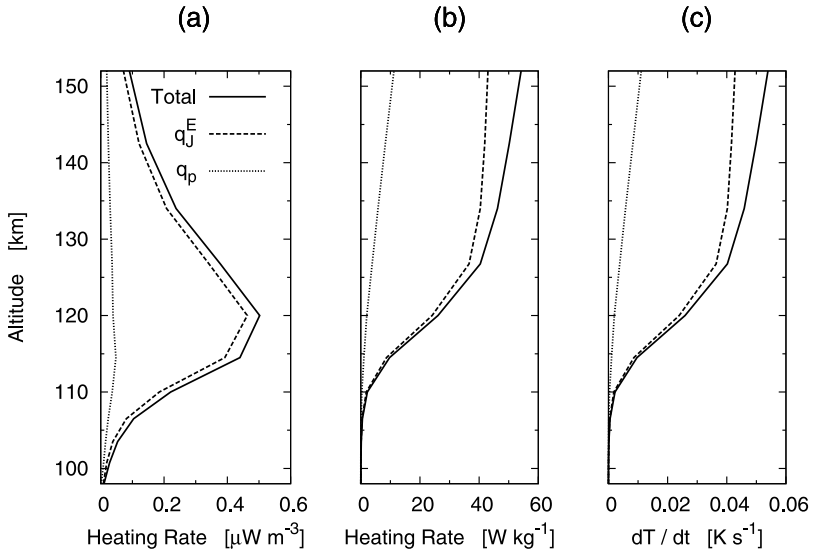

Figure 8. Altitude profiles of (a) the average auroral heating rates per unit volume (μW m^{-3}), (b) the average auroral heating rates per unit weight (W kg^{-1}), and (c) the average temperature increasing rates (K s^{-1}) from 00:03 to 00:33 UT. The dashed lines represent the passive energy deposition rate, the dotted lines represent the particle heating rate, and the solid lines represent their total heating rate.

launch, temperature enhancements expected from the observed temperature increase rate are calculated to be 4 K, 47 K, 77 K, and 86 K at 110 km, 120 km, 130 km, and 140 km, respectively. The estimated temperature enhancements are within the uncertainties of the observed temperature enhancements above 130 km but are much smaller below 120 km.

[35] As discussed in Section 4.1, the heating rates during 00:00–01:00 UT are suggested to be horizontally nonuniform within the measurement region of the EISCAT UHF radar. Furthermore, horizontal distances between the rocket trajectory above 100 km altitude and the EISCAT UHF radar site ranged from 120 to 130 km. Although there can be a difference between temperature enhancements estimated from the data taken with the EISCAT UHF radar and those taken with the rocket-borne instrument, a difference between altitude variations of the temperature enhancements can be caused by a reason other than the horizontal distance.

[36] In Section 3, the passive energy deposition rate was introduced as an alternative to the Joule heating rate by neglecting the neutral wind effect ($\mathbf{U} \times \mathbf{B}$). Since this assumption was validated with the neutral wind data from the FPI observation, it was concluded that the passive energy deposition rate is almost identical to the Joule heating rate for the data set analyzed in this paper. Nevertheless, it is important to consider the height-dependent neutral wind effect, $\mathbf{u} \times \mathbf{B}$, where $\mathbf{u}$ is the neutral wind speed at a specific altitude, because this term actually can either strengthen the Joule heating rate if $\mathbf{u} \times \mathbf{B}$ and $\mathbf{E}$ are parallel, or reduce the Joule heating rate if they are antiparallel [*Brekke et al.*, 1991; *Brekke*, 1997]. The horizontal wind speed estimated from the FPI observation is expected to correspond to the wind at a height where the green line emission has a peak, and the actual speed at a specific altitude can vary significantly. *Nozawa et al.* [2006] analyzed neutral winds observed with the EISCAT UHF radar during the campaign and derived semidiurnal tidal amplitudes and phases from 98 to 110 km altitudes. They found that the day-to-day variability of the semidiurnal tide was prominent for the amplitude and its peak altitude. The semidiurnal amplitude on the night of 12–13 December appeared to maximize at and below 104 km with a value of 100–120 m s^{-1}, and wind speeds during 00:00–01:00 UT on 13 December ranged from 0 to 200 m s^{-1}. If there was a wind speed of 200 m s^{-1} at any altitude under an electric field of 50 mV m^{-1}, it could either strengthen the Joule heating rate by up to 40% or reduce it by up to 33%, depending on the wind direction. By this means, the estimation of the Joule heating rate could be improved by observing neutral winds in the whole altitude range.

[37] It is notable that neutral density is one of the most important factors for the estimation of temperature increase rate in the lower thermosphere, especially below 120 km. As already mentioned in Section 3, the Joule and passive energy deposition rate below 110 km is inversely proportional to the neutral number density. Furthermore, the temperature increase rate in Equation (7) is derived by dividing the total heating rate by the neutral mass density. Therefore, temperature increase rate below 110 km can be proportional to the inverse square of the neutral density when the Joule heating prevails over the particle heating, and at least, the temperature increase rate is inversely proportional to the neutral density at all altitudes for either heating process. The same is true for the vertical wind speed estimation because vertical wind speed in Equation (6) is also derived by dividing the total heating rate by the neutral number density.

[38] In this study, the temperature enhancement is defined assuming the MSIS model neutral temperature as the ground state. On the other hand, the temperature increase rate is derived using the MSIS model neutral density, which is likely to be different from the ground state. *Kurihara et al.* [2006] reported that the N_2 number density observed simultaneously with the rotational temperature by the rocket-borne instrument is much lower than the MSIS model and changes with altitude from 30% of the MSIS model N_2 number

density at 95 km to 90% of that at 140 km. Their absolute density measurement may include systematic error caused by the aerodynamic effect, which cannot be easily corrected, but their relative density measurement is highly reliable. Their result suggests a relative decrease (increase) of neutral density in lower (higher) altitude. If the neutral density is 25% of the MSIS model N_2 number density at 110 km, the observed temperature enhancement can be explained only by a temperature increase rate due to the auroral heating effect. This neutral density decrease is also able to explain the observed large vertical wind. However, such a large decrease of the neutral density is unrealistic in the lower thermosphere even in highly disturbed conditions. Therefore, an additional mechanism is required to explain the observed temperature enhancements below 120 km.

5. Summary and Conclusions

[39] In this paper, temperature enhancements and upward vertical winds in the polar lower thermosphere associated with geomagnetic disturbance during the DELTA campaign were investigated. The height-resolved passive energy deposition rate and particle heating rate in the lower thermosphere were derived from the data taken with the EISCAT UHF radar and compared with the N_2 rotational temperature observed in situ by the rocket-borne instrument and with the vertical wind speed observed from the auroral green line emission by the ground-based FPI.

[40] The vertical winds seem to respond nearly instantaneously to changes in the heating rates and the wind speeds were associated with the height-integrated passive energy deposition rate and particle heating rate. A closer relationship with the passive energy deposition rate was found when the estimated height of vertical winds was about 120 km, likewise with the particle heating rate when the estimated height was about 110 km. The present study demonstrates that the observed vertical wind speed cannot be explained by the estimated heating rate and the thermal expansion hypothesis. It is suggested that the generation mechanism of large vertical winds must be responsible for the fast response of the vertical winds to an auroral heating event.

[41] The temperature enhancements defined by the difference between the observed N_2 rotational temperature and the MSISE-90 model value were uniformly 70–140 K at 110–140 km altitude. Neutral density is potentially important for understanding the dynamics and energetics in the polar lower thermosphere because equations of the vertical wind speed and temperature increase rate are function of the neutral density. However, the observed temperature enhancements below 120 km cannot be explained only by the neutral density effect.

[42] **Acknowledgments.** The authors thank all the staff of the Institute of Space and Astronautical Science and the Andoya Rocket Range for conducting the successful rocket experiment. The authors are indebted to the director and staff of the EISCAT for operating the facility and supplying the data. The EISCAT is an international association supported by research organizations in China (CRIRP), Finland (SA), France (CNRS, until the end of 2006), Germany (DFG), Japan (NIPR and STEL), Norway (NFR), Sweden (VR), and the United Kingdom (PPARC). The MIRACLE network is operated as an international collaboration under the leadership of the Finnish Meteorological Institute. The IMAGE magnetometer data are collected as a joint European collaboration. One of the authors (J.K.) is supported by Research Fellowships of the Japan Society for the Promotion of Science for Young Scientists. One of the authors (S.O.) was supported by grant 2007-1136 from Yamada Science Foundation. This research was partly supported by a grant-in-aid for Scientific Research B (16340146, 17340145, and 18403010) by the Ministry of Education, Culture, Sports, Science and Technology of Japan. This research was partially supported by the grant-in-aid for Nagoya University Global COE Program, "Quest for Fundamental Principles in the Universe: From Particles to the Solar System and the Cosmo," from the Ministry of Education, Culture, Sports, Science and Technology of Japan.

[43] Zuyin Pu thanks Mark Conde and another reviewer for their assistance in evaluating this manuscript.

References

Abe, T., J. Kurihara, N. Iwagami, S. Nozawa, Y. Ogawa, R. Fujii, H. Hayakawa, and K.-I. Oyama (2006), Dynamics and Energetics of the Lower Thermosphere in Aurora (DELTA)—Japanese sounding rocket campaign, *Earth Planets Space*, *58*, 1165–1171.

Aruliah, A. L., and D. Rees (1995), The trouble with thermospheric vertical winds: Geomagnetic, seasonal and solar cycle dependence at high latitudes, *J. Atmos. Terr. Phys.*, *57*, 597–609.

Banks, P. M., C. R. Chappell, and A. F. Nagy (1974), A new model for the interaction of auroral electrons with the atmosphere: Spectral degradation, backscatter, optical emission, and ionization, *J. Geophys. Res.*, *79*, 1459–1470.

Brekke, A. (1997), *Physics of the Upper Polar Atmosphere*, 491 pp., John Wiley, Chichester, U. K.

Brekke, A., and C. Hall (1988), Auroral ionospheric quiet summer time conductances, *Ann. Geophys.*, *6*, 361–376.

Brekke, A., and C. L. Rino (1978), High-resolution altitude profiles of the auroral zone energy dissipation due to ionospheric currents, *J. Geophys. Res.*, *83*, 2517–2524.

Brekke, A., J. Moen, and C. Hall (1991), Studies of the conductivities in the auroral zone ionosphere, *J. Geomag. Geoelectr.*, *43*, suppl., 441–465.

Crickmore, R. I., J. R. Dudeney, and A. S. Rodger (1991), Vertical thermospheric winds at the equatorward edge of the auroral oval, *J. Atmos. Terr. Phys.*, *33*, 483–492.

Deng, Y., and A. J. Ridley (2006a), Dependence of neutral winds on convection E-field, solar EUV, and auroral particle precipitation at high latitudes, *J. Geophys. Res.*, *111*, A09306, doi:10.1029/2005JA011368.

Deng, Y., and A. J. Ridley (2006b), Role of vertical ion convection in the high-latitude ionospheric plasma distribution, *J. Geophys. Res.*, *111*, A09314, doi:10.1029/2006JA011637.

Deng, Y., A. D. Richmond, A. J. Ridley, and H.-L. Liu (2008), Assessment of the non-hydrostatic effect on the upper atmosphere using a general circulation model (GCM), *Geophys. Res. Lett.*, *35*, L01104, doi:10.1029/2007GL032182.

Fujii, R., S. Nozawa, N. Matuura, and A. Brekke (1998), Study on neutral wind contribution to the electrodynamics in the polar ionosphere using EISCAT CP-1 data, *J. Geophys. Res.*, *103*, 14,731–14,739.

Fujii, R., S. Nozawa, S. C. Buchert, and A. Brekke (1999), Statistical characteristics of electromagnetic energy transfer between the magnetosphere, the ionosphere, and the thermosphere, *J. Geophys. Res.*, *104*, 2357–2365.

Fujiwara, H., S. Maeda, M. Suzuki, S. Nozawa, and H. Fukunishi (2004), Estimates of electromagnetic and turbulent energy dissipation rates under the existence of strong wind shears in the polar lower thermosphere from the European Incoherent Scatter (EISCAT) Svalbard radar observations, *J. Geophys. Res.*, *109*, A07306, doi:10.1029/2003JA010046.

Griffin, E., et al. (2006), Combined ground-based optical support for the aurora (DELTA) sounding rocket campaign, *Earth Planets Space*, *58*, 1113–1121.

Hays, P. B., R. A. Jones, and M. H. Rees (1973), Auroral heating and the composition of the neutral atmosphere, *Planet. Space Sci.*, *21*, 559–573.

Hedin, A. E. (1991), Extension of the MSIS thermosphere model into the middle and lower atmosphere, *J. Geophys. Res.*, *96*, 1159–1172.

Holmes, J. M., M. Conde, C. Deehr, and D. Lummerzheim (2005), Morphology of evening sector aurorae in λ557.7-nm Doppler temperatures, *Geophys. Res. Lett.*, *32*, L02103, doi:10.1029/2004GL021553.

Innis, J. L., P. L. Dyson, and P. A. Greet (1997), Further observations of the thermospheric vertical wind at the auroral oval/polar cap boundary, *J. Atmos. Sol. Terr. Phys.*, *59*, 2009–2022.

Ishii, M., S. Oyama, S. Nozawa, R. Fujii, E. Sagawa, S. Watari, and H. Shinagawa (1999), Dynamics of neutral wind in the polar region observed with two Fabry-Perot interferometers, *Earth Planets Space*, *51*, 833–844.

Ishii, M., M. Conde, R. W. Smith, M. Krynicki, E. Sagawa, and S. Watari (2001), Vertical wind observations with two Fabry-Perot interferometers at Poker Flat, Alaska, *J. Geophys. Res.*, *106*, 10,537–10,551.

Ishii, M., M. Kubota, M. Conde, R. W. Smith, and M. Krynicki (2004), Vertical wind distributions in the polar thermosphere during Horizontal E Region Experiment (HEX) campaign, *J. Geophys. Res.*, *109*, A12311, doi:10.1029/2004JA010657.

Iwagami, N., S. Komada, and T. Takahashi (2006), Preliminary results of rocket attitude and auroral green line emission rate in the DELTA campaign, *Earth Planets Space*, *58*, 1107–1111.

Kurihara, J., and K.-I. Oyama (2005), Rocket-borne instrument for measuring vibrational-rotational temperature and density in the lower thermosphere, *Rev. Sci. Instrum.*, *76*, 083101-1–083101-6, doi:10.1063/1.1988189.

Kurihara, J., T. Abe, K.-I. Oyama, E. Griffin, M. Kosch, A. Aruliah, K. Kauristie, Y. Ogawa, S. Komada, and N. Iwagami (2006), Observations of the lower thermospheric neutral temperature and density in the DELTA campaign, *Earth Planets Space*, *58*, 1123–1130.

Kofman, W., C. Lathuillere, and B. Pibaret (1996), Neutral dynamics of the high latitude *E* region from EISCAT measurements: A new approach, *J. Atmos. Terr. Phys.*, *58*, 121–138.

Kosch, M. J., M. Ishii, A. Kohsiek, D. Rees, K. Schlegel, T. Hagfors, and K. Cierpka (2000), Comparison of vertical thermospheric winds from Fabry-Perot interferometer measurements over a 50 km baseline, *Adv. Space Res.*, *26*, 985–988.

Nozawa, S., Y. Ogawa, A. Brekke, T. Tsuda, C. M. Hall, H. Miyaoka, J. Kurihara, T. Abe, and R. Fujii (2006), EISCAT observational results during the DELTA campaign, *Earth Planets Space*, *58*, 1183–1191.

Oyama, S., B. J. Watkins, S. Maeda, and J. Waterman (2005), Application of a new beam configuration to estimate lower thermospheric vertical velocities at high latitudes with monostatic incoherent scatter radars, *Radio Sci.*, *40*, RS4005, doi:10.1029/2004RS003205.

Oyama, S., B. J. Watkins, S. Maeda, H. Shinagawa, S. Nozawa, Y. Ogawa, A. Brekke, C. Lathuillere, and W. Kofman (2008), Generation of the lower-thermospheric vertical wind estimated with the EISCAT KST radar at high latitudes during periods of moderate geomagnetic disturbance, *Ann. Geophys.*, *26*, 1491–1505.

Price, G. D., and F. Jacka (1991), The influence of geomagnetic activity on the upper mesosphere/lower thermosphere in the auroral zone. part I. Vertical winds, *J. Atmos. Terr. Phys.*, *53*, 909–922.

Price, G. D., R. W. Smith, and G. Hernandes (1995), Simultaneous measurements of large vertical winds in the upper and lower thermosphere, *J. Atmos. Terr. Phys.*, *57*, 631–643.

Rees, D., R. W. Smith, P. J. Charleton, F. G. McCormac, N. Lloyd, and Å. Steen (1984), The generation of vertical winds and gravity waves at auroral latitudes, part I. Observations of vertical winds, *Planet. Space Sci.*, *38*, 667–684.

Russell, A. T., J.-P. St.-Maurice, R. J. Sica, and J.-M. Noël (2007), Composition changes during disturbed conditions: Are mass spectrometers overestimating the concentrations of atomic oxygen?, *Geophys. Res. Lett.*, *34*, L21106, doi:10.1029/2007GL030607.

Shinagawa, H., and S. Oyama (2006), A two-dimensional simulation of thermospheric vertical winds in the vicinity of an auroral arc, *Earth Planets Space*, *58*, 1173–1181.

Shinagawa, H., S. Oyama, S. Nozawa, S. C. Buchert, R. Fujii, and M. Ishii (2003), Thermospheric and ionospheric dynamics in the auroral region, *Adv. Space Res.*, *31*, 951–956.

Smith, R. W. (1998), Vertical winds: a tutorial, *J. Atmos. Sol. Terr. Phys.*, *60*, 1425–1434.

Smith, R. W. (2000), The global-scale effect of small-scale thermospheric disturbances, *J. Atmos. Sol. Terr. Phys.*, *62*, 1623–1628.

Smith, R. W., and G. Hernandez (1995), Vertical winds in the thermosphere with in the polar cap, *J. Atmos. Terr. Phys.*, *57*, 611–620.

Sun, Zi-Ping, R. P. Turco, R. L. Walterscheid, S. V. Venkateswaran, and P. W. Jones (1995), Thermospheric response to morningside diffuse aurora: High-resolution three-dimensional simulations, *J. Geophys. Res.*, *100*, 23,779–23,793.

Thayer, J. P. (1998a), Height-resolved Joule heating rates in the high-latitude *E* region and the influence of neutral winds, *J. Geophys. Res.*, *103*, 471–487.

Thayer, J. P. (1998b), Radar measurements of the electromagnetic energy rates associated with the dynamic ionospheric load/generator, *Geophys. Res. Lett.*, *25*, 469–472.

Thayer, J. P. (2000), High-latitude currents and their energy exchange with the ionosphere-thermosphere system, *J. Geophys. Res.*, *105*, 23,015–23,024.

Vickrey, J. F., R. R. Vondrak, and S. J. Matthews (1982), Energy deposition by precipitating particles and Joule dissipation in the auroral ionosphere, *J. Geophys. Res.*, *87*, 5184–5196.

Walterscheid, R. L., and L. R. Lyons (1992), The neutral circulation in the vicinity of a stable auroral arc, *J. Geophys. Res.*, *97*, 19,489–19,499.

Walterscheid, R. L., L. R. Lyons, and K. E. Taylor (1985), The perturbed neutral circulation in the vicinity of a symmetric stable auroral arc, *J. Geophys. Res.*, *90*, 12,235–12,248.

Wardill, P., and F. Jacka (1986), Vertical motions in the thermosphere over Mawson, Antarctica, *J. Atmos. Terr. Phys.*, *48*, 289–292.

Wescott, E. M., H. Stenbaek-Nielsen, M. Conde, M. Larsen, and D. Lummerzheim (2006), The HEX experiment: Determination of the neutral wind field from 120 to 185 km altitude near a stable premidnight auroral arc by triangulating the drift of rocket-deployed chemical trails, *J. Geophys. Res.*, *111*, A09302, doi:10.1029/2005JA011002.

T. Abe, Institute of Space and Astronautical Science, Japan Aerospace Exploration Agency, 3-1-1 Yoshinodai, Sagamihara, Kanagawa 229-8510, Japan.

A. Aruliah and E. Griffin, Atmospheric Physics Laboratory, University College London, 67-73 Riding House Street, London W1W 7EJ, UK.

R. Fujii, J. Kurihara, S. Nozawa, S. Oyama, and T. T. Tsuda, Solar-Terrestrial Environment Laboratory, Nagoya University, Furo-cho, Cikusa-ku, Nagoya 464-8601, Japan. (kuri@stelab.nagoya-u.ac.jp)

N. Iwagami, Department of Earth and Planetary Science, Graduate School of Science, University of Tokyo, 7-3-1 Hongo, Bunkyo-ku, Tokyo 113-0033, Japan.

K. Kauristie, Finnish Meteorological Institute, P. O. Box 503, FIN-00101, Helsinki, Finland.

M. J. Kosch, Communication Systems, Lancaster University, Lancaster LA1 4WA, UK.

H. Miyaoka and Y. Ogawa, National Institute of Polar Research, Research Organization of Information and Systems, 10-3 Midoricho, Tachikawa, Tokyo 190-8518, Japan.

K.-I. Oyama, Plasma and Space Science Center, National Cheng Kung University, 1 Ta-Hsueh Road, Tainan 70101, Taiwan.